IEEE Access
Multidisciplinary | Rapid Review | Open Access Journal

Received February 28, 2020, accepted March 20, 2020, date of publication April 8, 2020, date of current version April 22, 2020.

Digital Object Identifier 10.1109/ACCESS.2020.2986716

Angular Dispersion of a Scattered Underground Wireless Channel at 60 GHz

SHAH AHSANUZZAMAN MD TARIQ[1], CHARLES L. DESPINS[2], (Senior Member, IEEE), SOFIÈNE AFFES[3], (Senior Member, IEEE), AND CHAHÉ NERGUIZIAN[1], (Member, IEEE)

[1]Electrical Engineering Department, Université de Montréal-École Polytechnique, Montreal, QC H3T 1J4, Canada
[2]Electrical Engineering Department, Université du Québec-École de Technologie Supérieure, Montreal, QC H3C 1K3, Canada
[3]Electrical Engineering Department, Université du Québec-Institut National de la Recherche Scientifique, Montreal, QC H2X 2C6, Canada

Corresponding author: Shah Ahsanuzzaman Md Tariq (tariq.shah-ahsanuzzaman-md@polymtl.ca)

This work was supported in part by the NSERC, in part by the Bell Alliant, in part by the Newtrax CRD Project, and in part by the NSERC CREATE PERSWADE Program.

ABSTRACT The 60 GHz frequency band is identified as a suitable band for Gbps speed wireless communication in an Underground mine due to its high antenna directivity and high signal attenuation. However, the rough mine surface and the 5 mm wavelength may produce rich scattering phenomenon of multipath signals. To characterize the channel and more insight into the scattering, the angular dispersion measurements are conducted in different mine gallery depths and dimensions. The scattering is analyzed by the angle of arrivals of the incoming paths at the receiver, which is characterized by the statistical parameters of the multipath shape factors. The results of the multipath shape factor are explained and show that at around 3 m link distance, the incoming paths are mostly in two or three directions within a resolution angle of around between $\pm 30°$ and $\pm 40°$. The statistical distribution of the multipath angle of arrivals follows a Gaussian probability distribution. The results also show that the angular spreads of multipath are proportional to the gallery dimensions and inversely proportional to the link distances.

INDEX TERMS 60 GHz wideband channel measurements, underground mine, angle of arrivals, scattering.

I. INTRODUCTION

The 60 GHz frequency band has recently been studied and promoted in IEEE 802.15.3c, IEEE 802.11.ad, WirelessHD, ECMA-387 standards for short-range multi-gigabit per second speed wireless local area network WLAN) inside the room, office, vehicle and in outdoor as small cell backhaul [1]–[4]. It has a 7 GHz unlicensed bandwidth, high oxygen absorption loss, and fewer interference features compared to lower-frequency bands (e.g., < 6 GHz). Nowadays, the application of this frequency band is driving underground wireless low latency communication applications for mining industries nowadays to enhance mineral productions which may provide virtual reality (VR), real-time high definition (HD) video streaming, remote operation of mineral extraction and production, geolocalization of miners and vehicles with higher accuracy as well as robotic operations. For instance, a remotely controlled vehicle with a HD camera requires gigabit per second speed data transmission from the ground with a low latency feature that might be possible with 7 GHz bandwidth. The 60 GHz directive antenna system performing beamforming and which can be used efficiently for a 10 to 20 m Underground mine wireless network. For longer distances such as 150 m, it is also recommended to use of 60 GHz backhauling in the underground mine wireless network where the gallery curvatures and tilted walls act as obstacles. To deploy such network, antenna and system designers need to specify the antenna beam resolutions and angular characteristics. The wireless channel measurements are required since commercial wireless propagation simulation tools are not compatible with these kinds of hazard environments.

For more than a decade, the Laboratoire de recherche Télébec en communications souterraines (LRTCS) - Université du Québec en Abitibi - Témiscamingue (UQAT) laboratory, located in Val-d'Or, Canada, has performed measurements in order to improve mining industry wireless communication systems with different frequencies, galleries, and setups [5]–[10]. The experimental mine named Canada Centre for Mineral and Energy Technology (CANMET)

The associate editor coordinating the review of this manuscript and approving it for publication was Yuan Gao.

has been used for these measurement campaigns. The mine environment is different from offices and corridors since it consists of galleries with rough surfaces which can cause particular scattering at a wavelength of 5 mm. Angular dispersion characteristics of the scattered channel are highly relevant in that particular wavelength in the underground mine. The results of CANMET mine show that as the operating frequency increases and as the antenna half-power beamwidth (HPBW) decreases, a lower value of root mean square (RMS) delay spread is obtained. The value of RMS delay spread particularly depends on the antenna HPBW, the topology of the experiment, gallery curvature, and the operating wavelength as well as the transmitter-receiver separation (Tx - Rx) distances.

Experiments of the angle of arrival (AoA) have been reported in the literature for the indoor environment in different frequencies [11]–[14]. At 60 GHz, Xu *et al.* [11] reported that multipath comes along the line of sight (LOS) direction in the hallway and the angular spread is smaller than the one in the rooms. At 7 GHz, Spencer *et al.* [12] observed that the multipath angle of arrivals in a cluster have a Laplacian distribution with standard deviations of angular spread of 22° to 26°. Loni *et al.* [13] noted that the angular spread values for indoor environments are higher than those for outdoor environments, showing that multipath comes from multiple directions in an indoor environment. Moreover, Moraitis *et al.* [14] reported that the AoA shape factors which characterize multipath AoA in an indoor environment relate to a specific area and correlate between the environment and the multipath channel structure. In outdoor urban environments, the RMS lobe azimuth spread at 28 GHz is found to be 6° [1]. However, several experiments have been conducted in CANMET underground mine at 60 GHz frequency and the time dispersion, scattering analysis, statistical modeling, antenna polarization effect results are reported recently in [15]–[18]. The angle of arrival results are disclosed herein and in the Ph.D. thesis of the first author [19]. The main contributions of this article are presenting the 60 GHz AoA measurement results and analysis those were conducted in different mine gallery level depths.

II. MEASUREMENT SETUP AND EXPERIMENTAL PROTOCOL

In the CANMET experimental mine, two measurements zones at 40 m and 70 m gallery level depths were used. The dimensions of the mine galleries at both levels are listed in Table 1. The 70 m depth gallery was dustier than 40 m gallery and the floor was covered with water puddles. At 70m, the floor was mostly flat and consisted of small rock tiles. Gallery walls at both depths were mostly rough and consisted of sharp edges. The estimated roughness was 6 cm at 40 m depth [18] and a little less at the 70 m level (according to visual observation, no experimental data available so far). The humidity and the temperature of both galleries were 100 percent and 6 degrees Celsius, respectively. Digital photographs of the two underground mine galleries are shown in Fig. 1.

TABLE 1. Approximate dimensions of the Val-d'Or, CANMET Underground mine Galleries.

Depth (m)	Height (m)	Width (m)	Length (m)
40	5	5	30
70	2.5-3	3	70

Note: The value of the length is an approximate straight line of sight distance before a curvature [5], [7].

(a)

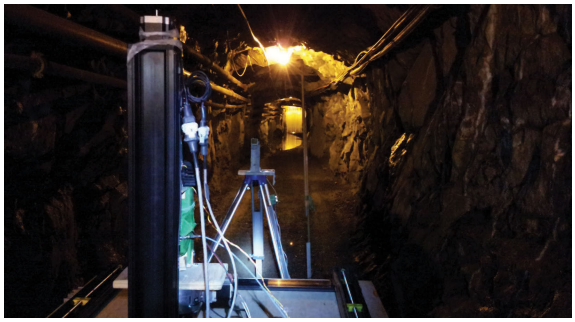

(b)

FIGURE 1. (a) 40 m and (b) 70 m level depth gallery.

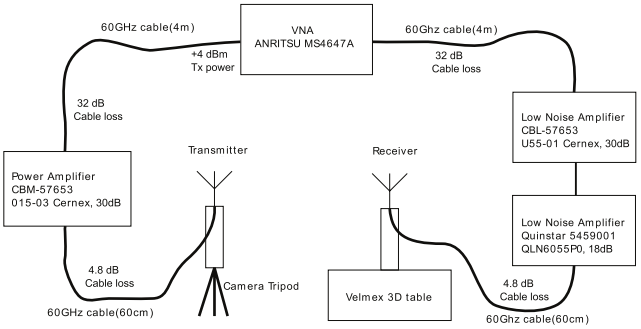

FIGURE 2. Experimental setup.

In order to find channel frequency response $H(f)$, a 60 GHz frequency domain wideband measurement system setup with a Vector Network Analyzer (VNA-ANRITSU MS 4647A) was used. The schematic diagram of the experimental setup is shown in Fig. 2 and the measurement parameters are listed in Table 2. The SOLT (short-open-load-thru) calibration was done with 2000 frequency sweep points with a sampling frequency of 1.08 MHz. A camera tripod and a laser were used during measurements of the wireless channel in order

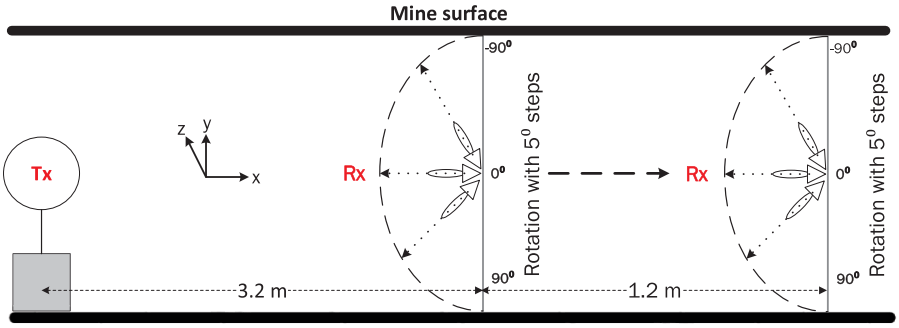

FIGURE 3. AoA measurement procedure with Omnidirectional antenna at the Tx and directional Horn antenna at the Rx.

TABLE 2. Parameters of 60 GHz channel measurements.

Mine Level	40 m, 70 m
Frequency range	57.24 GHz-59.4 GHz
Bandwidth	2.16 GHz
Tx power	+4 dBm
Angular; Tx/Rx height	1.42 m
Temporal; Tx/Rx height	1.5 m
Sweep points	2000
Sampling frequency	1.08 MHz
Power amplifier gain	30 dB
Low noise amplifier gain	18 dB and 30 dB
Pyramidal Horn antenna	Gain 24 dBi, HPBW 12°
Omnidirectional antenna	Gain 3 dBi
Polarization	VV
60 GHz cable loss	7.86 dB/m

to have the accurate visibility of the LOS condition. The data acquisition was completed by connecting a computer to the VNA via a GPIB (General Purpose Interface Bus) interface. A Velmex table having the capability to do the 3D measurement was used to move the Rx along the x, y, z directions simultaneously and accurately. LabVIEW and MATLAB programs were employed to record data and to control the whole measurement procedure, respectively.

1) ANGULAR DISPERSION MEASUREMENTS

During Angle of Arrival (AoA) measurements in the 70 m gallery, the Rx was moved from 3.2 m to 4.4 m along the x-axis as shown in Fig. 3. The separation between two successive positions was 40λ. At 40 m gallery, the Rx moved from 3 m to 4 m (separated by 1 m) along the x-axis. A 1 m reference measurement was used to remove the antenna side lobe effect and the system losses so-called over the air (OTA) calibration. Along the elevation direction (i.e. z-axis), six consecutive measurements were taken at each position separated by $\lambda/2$ to have an average of spatial fading and to reduce the antenna misalignment issue (caused by the rough floor). At each position, 15 snapshots for different time instances were recorded in order to have a local average which eliminates the time-varying small-scale fading.

During measurements campaign of both galleries, an attenuation of the reflected waves was observed approximately between 3 m and 4 m from the Tx. Moreover, the length of the linear track in the Velmex table was around 1.5 m. For these two reasons, AoA measurements in both galleries campaigned around between 3 m and 4 m from the Tx. At each position, the Rx was moved in azimuth directions from −90° to 90° with a step of 5° with an accurate programmable Velmex linear track in order to have the azimuthal coverage of 180°. An HPBW for the rotational antenna is larger than the step size (5°) of the measurement which offers a sufficient angular space to receive a strong multipath at the Rx. These measurements were conducted particularly to evaluate the scattering effect and also to obtain the angular characteristics of the multipath.

A. POST PROCESSING PROCEDURE

Firstly, during angular dispersion measurements, the 37 frequency responses were obtained at each position by averaging 15 snapshots. Therefore, 1776 (8 and 6 positions along the x-axis and z-axis, respectively) and 666 (3 and 6 positions along the x-axis and z-axis, respectively) frequency responses were stored for post-processing to investigate the multipath arrivals at 70 m and 40 m gallery, respectively. Secondly, the OTA calibration of data was performed by dividing 1 m complex-valued frequency response with all complex-valued frequency responses of the measurements. Finally, using the Inverse Fast Fourier Transform (IFFT), the normalized channel impulse responses with a 0.46 ns time resolution were obtained from the OTA calibrated frequency responses using the procedure employed in [7]. Therefore, for a position d and delay τ, the channel impulse responses $h(\tau; d)$ were obtained leading to the Power Delay Profiles (PDPs) calculated by $P(\tau; d) = |h(\tau; d)|^2$. The threshold level of noise was followed according to the procedure described in [20]. An example of a PDP post-processing is shown in Fig. 4. The peaks and inflections were indicated as paths. A gradual decrement of the power of the paths was observed once the delay increases. Inflections were chosen because the scattering from the rough surface may contribute two consecutive paths arriving within a very small difference of the delay.

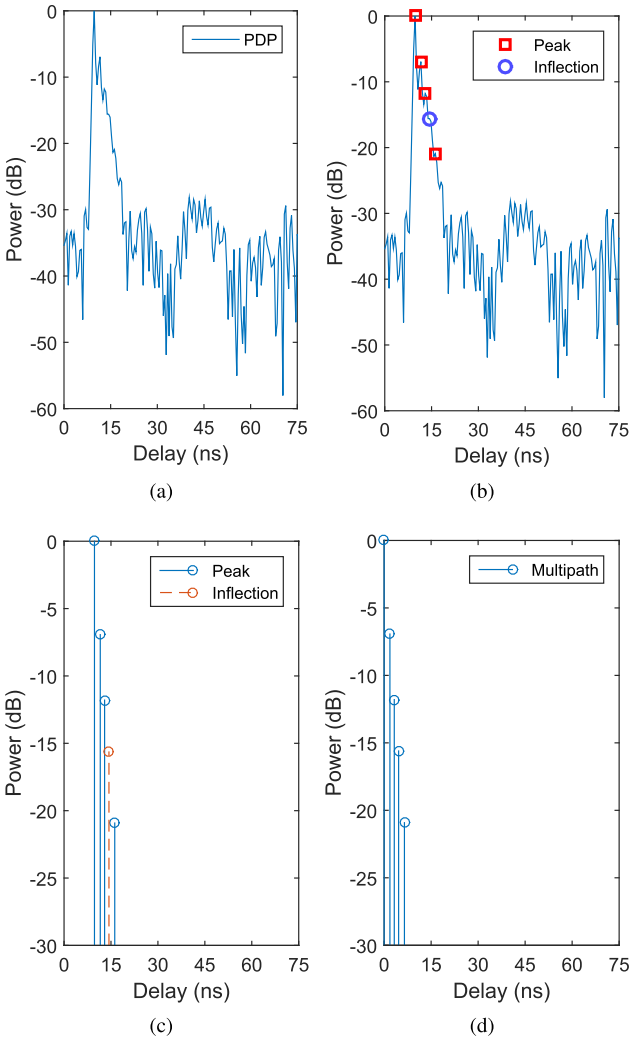

FIGURE 4. An example of a PDP post processing. (a) the recorded signal, (b) peaks and inflection detection, (c) detected LOS path and multipath, and (d) shifted power delay profile.

III. ANGULAR DISPERSION CHARACTERISTICS

This section investigates the angular characteristics of the channel in the 70 m and 40 m level galleries. The multipath shape factors are introduced by the angular distribution of the multipath power $p(\theta)$ where θ is the angle of measurements. Statistical modeling of the angle of arrivals of an indoor multipath channel has been reported in [12]. In [11] and [21], the theory and experimental results of multipath shape factors such as the angular spread (Λ), angular constriction (γ), direction of maximum fading (θ_{max}) and maximum AoA direction of the angular distribution of the multipath power have been described. Shape factor theory has been considered herein since it can provide more information on multipath arrivals where scattering is of high concern. The extension of this theory is reported in [29] and [30] which may be used to characterize the dispersion of multipath energy in both azimuth and elevation planes as jointly or independently. The shape factor parameters were extracted from the recorded Power Angular Profiles (PAPs) in order to characterize the distribution of the multipath power and to investigate reflection and scattering phenomena in the galleries. First, the individual amplitude (a) and delay (τ) from the channel impulse response $h(\tau)$ have been extracted. Second, at a certain distance, the average values of PAPs have been calculated as [11], [14]

$$p(\theta) = \frac{1}{M}\sum_{k=1}^{M}\left(\sum_{i=1}^{N}|a_i(\theta, z_k)|^2\,\delta\left\{\tau - \tau_i(\theta, z_k)\right\}\right) \quad (1)$$

where M and N are the number of measurement points along the z direction denoted as z_k ($k = 1, 2, \ldots, 6$) and the number of sweep points ($i = 1, 2, \ldots, 2000$), respectively. The values of θ range used from $-\pi/2$ to $\pi/2$ with 5° angular resolution.

Angular spread (Λ) characterizes the multipath power by the ranges from zero to one. A value of zero represents one single path from a single direction and a value close to unity denotes multipath coming from multiple directions. The angular constriction (γ) specifies how multipath components are distributed along with the two directions (towards $-90°$ and 90° from 0°). Maximum fading angle (θ_{max}) provides the azimuthal direction of maximum fading in which Rx will not receive multipath components in that direction. Maximum AoA represents the angular direction of the strongest multipath component at the Rx. The adjacent spread of power arriving in the azimuth or elevation directions can be defined as a lobe [22]. The azimuth and elevation lobes can be different and depend on the antenna radiation patterns which define a propagation route.

A. RESULTS AND DISCUSSIONS

The underground mine surface is rough and consists of sharp rock edges. Hence the shape of each PAP is affected particularly by the grazing angles (i.e., around ±30°) of the multipath. Sharp rock edges may produce strong multipath on azimuth and elevation directions where the magnitude of the surface roughness is less than the 5 mm wavelength. Currently, there are no PAP experiments carried out for other frequencies such as 2.4 GHz and 5.8 GHz in CANMET mine but it is assumed that the multipath profile would be different at lower frequencies since its behavior depends on the operating frequency and the magnitude of the roughness.

1) 70 m GALLERY RESULTS

The PAPs and extracted multipath shape factor values at each distance are shown in Fig. 5 and listed in Table 3, respectively. For a fixed distance, the obtained lobes were constituted by the average (6 points along the z-direction × 15 snapshots) of 90 PAPs. According to the observation and analysis of multipath arrivals of 7 PAPs results, scattering exists in the underground mine environment and the PAPs will differ from those obtained from the simulations with the smooth surface.

To explain the scattering phenomenon, a comparison of multipath arrivals between rough and smooth surfaces were considered. By using the Wireless InSite software, a simulation scenario with a rectangular straight tunnel of 3 m width and 2 m height was carried out. The simulation param-

TABLE 3. AoA statistical parameters of 70 m gallery according to Tx - Rx distances. Λ and γ are dimensionless, θ_{max}, max AoA and Lobe angles are in degree, Peak Avg. values are in dB.

Distance	Λ	γ	θ_{max}	max AoA	Lobe angles	Peak Avg.
3.2 m	0.3063	0.8532	-89	-5	-49.99, -27.48, 0.54, 30.78	7.34
3.4 m	0.2950	0.8603	-83	-5	0.40, 36.17	7.87
3.6 m	0.2481	0.8539	84	-5	-38.11, 3.42, 35	8
3.8 m	0.2450	0.8926	89	-5	-38.45, 2.93, 31.5	8.13
4 m	0.2347	0.9069	87	10	-36.15, 0.82	8.79
4.2 m	0.2955	0.8527	-86	10	-33.56, 1.01, 31.44	7.84
4.4 m	0.3038	0.9069	82	-5	-36.18, 1.37, 27.57, 40	7.63

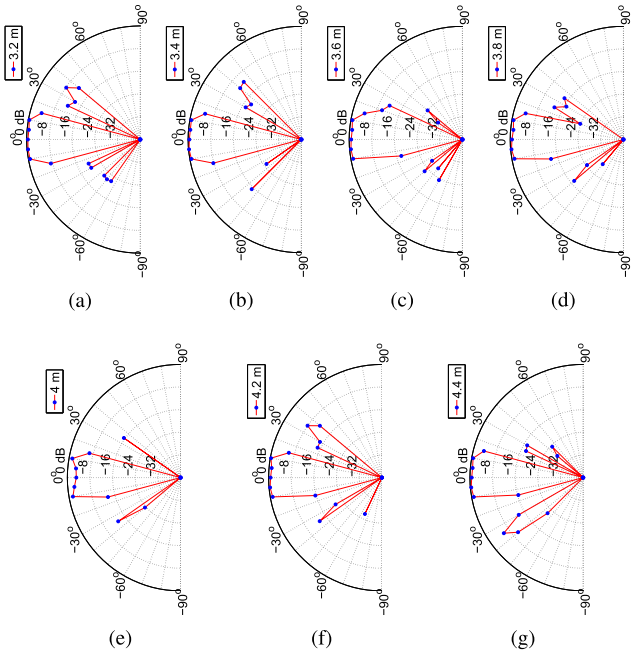

FIGURE 5. Normalized PAPs according to Tx - Rx distance of 3.2 m to 4.4 m with a step of 40λ at 70 m gallery.

eters and the protocols were same as the ones used in the experiments where an Omni - Omni antenna configuration was considered (during measurements, the horn antenna at the receiver has been rotated with 5° step). The surface roughness value was set to zero. Specular reflections and diffractions were considered for simulation purposes. The material properties were as defined in [23]. The comparison of the measured and simulated PAP results as shown in Fig. 6 that a difference of the multipath angle of arrivals within the short distance exists between the choice of smooth and rough surfaces implying the existence of scattering in the underground mine environment. As such, the roughness of the surface produces scattering, changing the amplitudes and the angles of multipath arrivals along the x, y and z directions of Rx. Due to time constraints, the angular measurements along the y-direction were not conducted. It has been observed for each PAP that the probability of having a multipath and an amplitude, at each specific angle, is random.

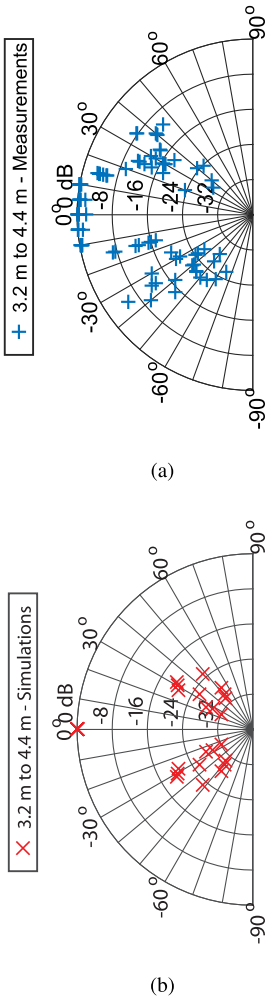

FIGURE 6. Normalized measured and simulated PAPs at 70 m level gallery. a) and (b) measured with rough surface (around 6 cm on magnitude) and simulated with smooth surface (zero roughness), respectively.

Measurement results show a small change in the values of Λ with the distance particularly due to the straight vein of the gallery. Its value lies between 0.2347 and 0.3038 within a 3.2 m to 4.4 m link distance, which corresponds to a range of values of Λ close to zero suggesting that the multipath does not come from multiple directions (coming only from two or three directions and not from one direction). Moreover,

it has been observed that within a 40λ distance (for example, at 3.4 m and 3.6 m distance in Fig 5b and 5c), the value of Λ varies, referring to the deviation of path arrivals caused by the surface roughness. As the reference, the experimental results in an indoor environment reflect our results as reported in [11], in which the multipath is accumulated in the main lobe, giving rise of a similar trend of angular spread values once the Rx location is closer to Tx.

As an example, geometrical analysis of Fig. 5 by considering a smooth surface shows that at a distance of 3.2 m with a fixed height of 3 m, the reflected path from the wall may have traveled 3.88 m and 4.38 m distances with respective angles of ±34° and ±42.92° corresponding to mine gallery widths of 2.2 m and 3 m, respectively. The measurement results show that the dominant lobe (consisting of several paths) is arriving along the LOS direction within a resolution angle of ±30° while the other three lobes (consisting also of several paths) arrived at angles of −49°, −27° and 30°. These lobe arrivals results show a difference with the ray propagation geometry where a smooth surface is considered. Accordingly, at a distance of 3.4 m, only one strong reflected dominant lobe arriving at an angle of 36° caused by the metallic pipe of the gallery as shown in Fig. 1b.

Angular constriction (γ) values are close to the value of 1 which indicates that multipath power is distributed around in both directions of the main lobe. These results are attributed to the rough walls, ceiling, and floor, and correspond to strong reflected waves arriving from angles corresponding to approximately ±30° (towards −90° and +90° from LOS angle) compared to the dominant path as shown in Fig. 5.

Maximum fading angle (θ_{max}), results show that values with variation, according to Tx - Rx distance caused by the rough surface of the gallery. At a distance of 4.2 m as seen in Fig. 5f, the maximum fading is almost perpendicular to the LOS path, since the maximum power of the multipath consists of a lobe of +31.44°. By considering the vector sum of multipath power, the maximum fading angle would be −86°.

For maximum AoA results show that its value lies between −5° and ±10° which is obvious at short Tx - Rx distance. Observations at each λ/2 separation distance along the z-axis also indicate that the values of maximum AoA are not varying significantly compared to the results obtained in Table 3. This is to note that, some lobes and paths (as shown in Figs. 5c and 5f) lie between 60° and 65°, indicating the scattering or diffraction phenomenon on the interaction points of the rough surface when the surface is close to the Rx which yields to a larger AoA.

The peak of the strongest multipath power is deduced from all pointing angles of the Rx. The ratio between maximum power and average multipath power is defined as the peak avg. and listed in Table 3. The received power of the dominant path (along with the LOS) does not change significantly and is around 5 dB. At a distance of 3.2 m and 3.4 m (Figs. 5a and 5b) the power at the positive link lobe of 30° remains almost the same, but at the 3.6 m location,

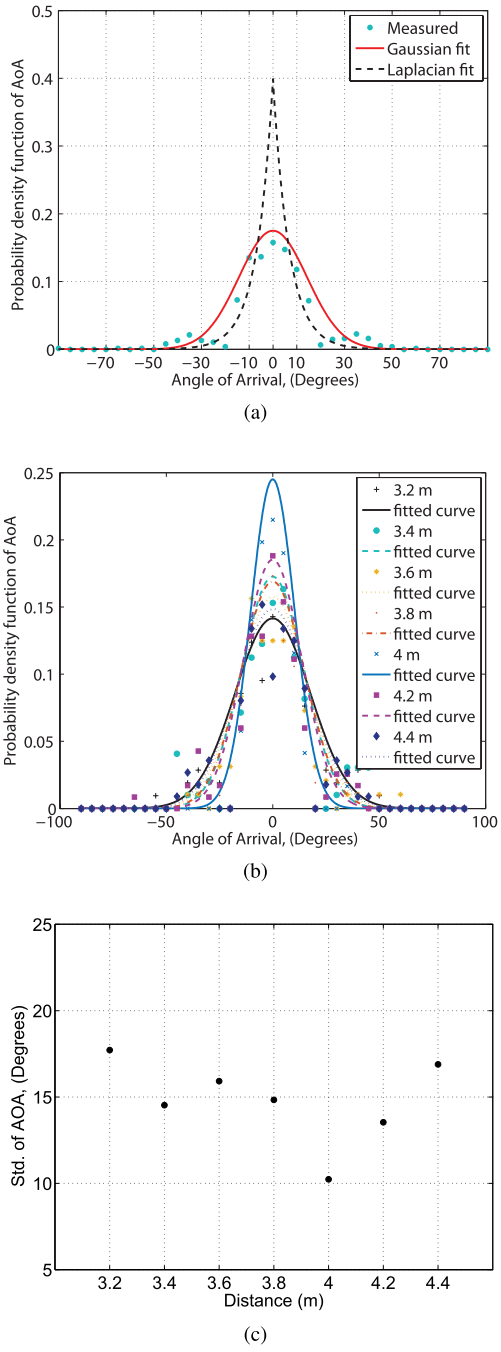

FIGURE 7. Distribution fitting of relative path arrivals with respect to angles at 70 m gallery. Superimposed by the best fit Gaussian distribution (σ_θ = 14.33°) is illustrated in (a), (b) illustrates the Gaussian distribution fitting of 7 PAPs of different distances and (c) illustrates the standard deviations of AoAs according to Tx - Rx distances.

the power degrades to around 14 dB. This is to note that two or three side lobes and those paths arrived around ±30° and one main lobe which consists of several paths arrived around ±15°.

The distribution of path arrivals with respect to angles extracted from 42 PAPs (6 points along the z-axis × 7 points along the x-axis) is shown in Fig. 7a. Zero mean Laplacian and Gaussian distributions fittings provide the standard

TABLE 4. AoA statistical parameters of 40 m gallery according to Tx - Rx distances. Λ and γ are dimensionless, θ, max AoA, and Lobe angles are in degree, Peak Avg. values are in dB.

Distance	Λ	γ	θ_{max}	max AoA	Lobe angles	Peak Avg.
3 m	0.3890	0.7684	78.9464	5	-76.14, -53.40, -2.99, 43.87	8.6639
4 m	0.1722	0.9707	88.60	0	0.0327	10.10

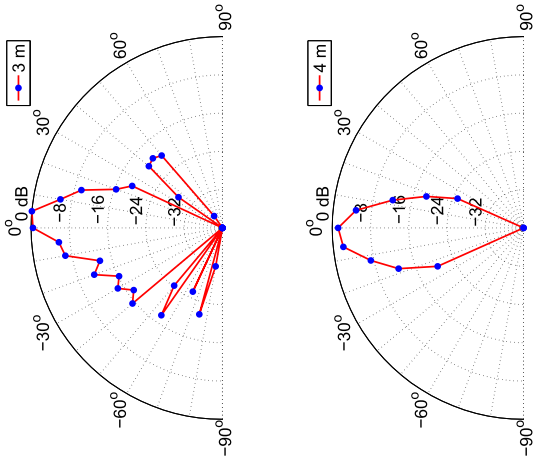

FIGURE 8. Normalized PAPs according to the Tx - Rx distance of 3 m and 4 m at 40 m gallery.

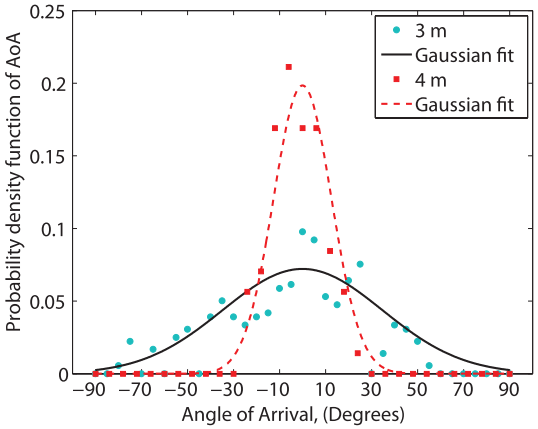

FIGURE 9. Gaussian distribution fitting, $\sigma_\theta = 34.75°$ at 3 m and $\sigma_\theta = 12.63°$ at 4 m.

deviations (defined as an angular spread, σ_θ) of 9.66° and 14.33°, respectively. Curve fitting, uses the least square method, closely matches with the Gaussian distribution. The Laplacian Probability Density Function (PDF) peak at 0° (AoA) is much higher than the Gaussian peak and does not correspond to the measured PDF (number of occurrences of path arrival angles). It indicates that the number of occurrences of path arrivals within that angle is not too high and does not consist of a sharp peak caused by the scattering.

This is to note that, an extension of the Saleh-Valenzuela (S-V) model introduced by Spencer [12] shows that the angle of arrival within a multipath cluster is assumed to have a zero-mean Laplacian distribution. Moreover, Zhang *et al.* [24] observed that the azimuth AoA follows a Laplacian distribution and the elevation AoA follows a Gaussian distribution in indoor environments. Nawaz *et al.* [30] discussed that the propagation environment like tunnels and streets may lead to a truncated AoA distribution caused by the physical dimensions. It is noted as well that the factors contributing to truncation causing symmetric or non-symmetric and isotropic or non-isotropic scattering of multipath waves.

At each distance, the Gaussian distribution fitting and the corresponding AoA standard deviation values are shown in Fig. 7b and 7c. The results show that when the distance increases, the value of the standard deviation becomes smaller due to a larger incident angle implying a lower value of σ_θ and tends to be smaller at farther distances along the x-direction of the gallery.

2) 40 m GALLERY RESULTS

Fig. 8 illustrates the average PAPs at 3 m and 4 m Tx - Rx distance. Results show that a wider gallery dimension provides a larger angular spread of multipath arrivals by comparing 40 m and 70 m results. As well, due to the higher value of incident angles, the larger Tx - Rx distance of 4 m provides the less angular spread of multipath arrivals as shown in Fig. 8b. The extracted statistical parameters of AoA are listed in Table 4.

Geometrically, with a Tx - Rx distance of 3 m, the reflected path could travel 5.8 m with an arrival angle of $\pm 59°$, but due to scattering and diffraction phenomena in the wider gallery, multipath arrived with large angles and the lobe angles are around 43°, $-53°$ and $-76°$. The angular constriction value at 3 m is lower than the 70 m level gallery (at 3.2 m) indicating that multipath power is distributed more in different directions. Gaussian curve fitting provides the standard deviations of 34.75° and 12.63° for the angle of arrivals at 3 m and 4 m as shown in Fig. 9, respectively. Moreover, the angular spread of the LOS lobe of the 40 m gallery is larger than at the one at 70 m gallery indicating that more multipath is arriving in different directions. At 4 m Tx - Rx distance, no side lobes were observed which indicates that all multipath are concentrated along the LOS direction and yields a higher peak average value. In addition, since side lobes at 3 m consist higher signal power attenuation which may provide an absence of multipath or a lobe at the receiver for higher traveling distance which has been actually obtained at 4 m link.

The comparison results between the indoor and underground mine measurement are listed in Table 5. The results indicate that a lower value of Λ observed in underground

TABLE 5. A comparison with different angle of arrival results conducted in the indoor and mine.

Reference	Environment	H (m)	W (m)	L(m)	Fc (GHz)	BW (GHz)	A_{tx}	A_{rx}	Tx - Rx	A_{tg}	A_{rg}	Λ
[11]	Indoor (room)	4.3	5.9	6.7	60 GHz	0.2	Waveguide	Horn	5.2	6.7	29	0.73
[11]	Indoor (Corridor)	4.3	2.9	54.7	60 GHz	0.2	Waveguide	Horn	5	6.7	29	0.48
In this work	CANMET (40 m depth)	5	5	30	58.32 GHz	2.16	Omni	Horn	3	3	24	0.38
In this work	CANMET (70 m depth)	2.5-3	3	70	58.32 GHz	2.16	Omni	Horn	3.2	3	24	0.30

Note: Fc and BW are the center frequency and bandwidth in GHz, respectively. A_{tx} and A_{rx} are the transmitter (Tx) and receiver (Rx) antenna types, respectively. Tx - Rx is the maximum transmitter-receiver separation distance in meter. A_{tg} and A_{rg} are the Tx and Rx antenna gains in dBi, respectively.

TABLE 6. A comparison with different angle of arrival results conducted in the tunnels and mine.

Location	Environment	H (m)	W (m)	F (GHz)	Method/Experiment	Angular spread
[25]	Underground mine (small tunnel)	5.1	3.8	2.8-5	Multimode Model	15.3° (10 - 50 m)
[25]–[27]*	2 way tunnel (large subway tunnel)	6.1	8.6	2.8 - 5	Experiment (roughness around 1 cm)	10° (50 m), 3° (200 m)
CANMET **	40 m depth	5	5	57.24 - 59.4	Experiment (roughness around 6 cm)	34.75°(3 m), 12° (4m)
CANMET **	70 m depth	2.5 - 3	3	57.24 - 59.4	Experiment	14.3° (3.2 m - 4 m)

Note: H is the height, W is the width, F is the frequency.
* Angular power spectrum theory was used to calculate angular spread as in [28] page 121 and in [26].
** The angles of multipath arrival fit with the Gaussian distribution and σ_θ was used to calculate the value of angular spread [12].

mine environment due to the higher value of the roughness magnitude where scattering phenomenon produces higher multipath signal power attenuations according to Tx - Rx distances.

Forooshani *et al.* [27] characterized the angular spread of different tunnel sizes and noted that the power- azimuth spectrum followed by a zero-mean Gaussian distribution. Also mentioned that the standard deviation of the angular spread is dependent on the tunnel dimension and the Tx - Rx distances. Moreover, Forooshani *et al.* [25] reported the angular spread of 10° and 3° at 50 m and 200 m link distances (i.e., the roughness of the surface is less than 1 cm and much lower than the wavelength) at a lower frequency, respectively. Results also identified that the angular spread becomes insignificant at higher Tx - Rx distance. A comparison with our experiments is indeed relevant since the operating frequency, the tunnel dimensions and the roughness of the surface are different (as the parameters to be considered for short range link distances) and listed in Table 6. It is noted that the angular spread decreases sharply as the distance increases as reported in [26] (i.e., 30° to 13°) at 10 to 50 m and as given in CANMET 40 m gallery results (i.e., 34.75° to 12° at 3 to 4 m). In contrast, at closer distances around 1 - 10 m, the angular spread becomes larger with larger gallery dimensions and its value depends on operating wavelength as well as on the surface roughness.

IV. CONCLUSION

This paper presents a measurement campaign concerning the angular characterization of a scattered wireless channel at 60 GHz. The results show that the multipath arrivals from different angular directions along the LOS (i.e., around $\pm 30°$) and multipath characteristics are different from those found on a smooth surface due to the scattering caused by the rough surfaces. The standard deviation of the path arrival distribution with respect to the angles was found to be around 18° (at 3.2 m) and 34° (at 3 m) in the 70 m and the 40 m galleries, respectively. Results show that a larger gallery dimension provides a higher value of the angular spread. In contrast, results suggest that a directional narrow beamwidth (i.e., $< 10°$) with directive - directive antenna (at the Tx and the Rx sides) system with a beam alignment, is essential for point to point backhaul links in the underground mine environment. The antenna beam steering may useful to align with the useful path due to the gallery curvature (to get a maximum power at a recovery link) at the Rx within a very short distance (i.e., around < 4 m).

The experiment particularly provides a better knowledge of angular resolution of 60 GHz antennas, the number of radio links and the lobe angles. The radio link designer may need to contemplate on the reflected lobe angles which can act as a successful recovery link, and on the rate of increments or decrements of angular spread according to the gallery dimensions and the link distances.

REFERENCES

[1] T. Rappaport, R. Heath, R. Daniels, and J. Murdock, *Millimeter Wave Wireless Communications* (Prentice-Hall Communications Engineering and Emerging Technologies Series). Upper Saddle River, NJ, USA: Prentice-Hall, 2014.

[2] S. K. Yong, P. Xia, and A. V. Garcia, *60 GHz Technology for Gbps WLAN and WPAN: From Theory to Practice*. Hoboken, NJ, USA: Wiley, 2011.

[3] P. F. M. Smulders, "Statistical characterization of 60-GHz indoor radio channels," *IEEE Trans. Antennas Propag.*, vol. 57, no. 10, pp. 2820–2829, Oct. 2009.

[4] M. Peter, R. Felbecker, W. Keusgen, and J. Hillebrand, "Measurement-based investigation of 60 GHz broadband transmission for wireless in-car communication," in *Proc. IEEE 70th Veh. Technol. Conf. Fall*, Anchorage, AK, USA, Sep. 2009, pp. 1–5.

[5] C. Nerguizian, C. L. Despins, S. Affes, and M. Djadel, "Radio-channel characterization of an underground mine at 2.4 GHz," *IEEE Trans. Wireless Commun.*, vol. 4, no. 5, pp. 2441–2453, Sep. 2005.
[6] Y. Rissafi, L. Talbi, and M. Ghaddar, "Experimental characterization of an UWB propagation channel in underground mines," *IEEE Trans. Antennas Propag.*, vol. 60, no. 1, pp. 240–246, Jan. 2012.
[7] M. Boutin, A. Benzakour, C. L. Despins, and S. Affes, "Radio wave characterization and modeling in underground mine tunnels," *IEEE Trans. Antennas Propag.*, vol. 56, no. 2, pp. 540–549, 2008.
[8] I. Ben Mabrouk, J. Hautcoeur, L. Talbi, M. Nedil, and K. Hettak, "Feasibility of a millimeter-wave MIMO system for short-range wireless communications in an underground gold mine," *IEEE Trans. Antennas Propag.*, vol. 61, no. 8, pp. 4296–4305, Aug. 2013.
[9] N. Hakem, G. Delisle, and Y. Coulibaly, "Radio-wave propagation into an underground mine environment at 2.4 GHz, 5.8 GHz and 60 GHz," in *Proc. 8th Eur. Conf. Antennas Propag. (EuCAP)*, Apr. 2014, pp. 3592–3595.
[10] M. Ghaddar, T. A. Denidni, L. Talbi, I. Ben Mabrouk, and M. Nedil, "Mm-waves propagation measurements in underground mine using directional MIMO antennas," *IET Microw., Antennas Propag.*, vol. 10, no. 5, pp. 517–524, Apr. 2016.
[11] H. Xu, V. Kukshya, and T. S. Rappaport, "Spatial and temporal characteristics of 60-GHz indoor channels," *IEEE J. Sel. Areas Commun.*, vol. 20, no. 3, pp. 620–630, Apr. 2002.
[12] Q. H. Spencer, B. D. Jeffs, M. A. Jensen, and A. L. Swindlehurst, "Modeling the statistical time and angle of arrival characteristics of an indoor multipath channel," *IEEE J. Sel. Areas Commun.*, vol. 18, no. 3, pp. 347–360, Mar. 2000.
[13] Z. M. Loni, R. Ullah, and N. M. Khan, "Analysis of fading statistics based on angle of arrival measurements," in *Proc. Int. Workshop Antenna Technol. (iWAT)*, Mar. 2011, pp. 314–319.
[14] N. Moraitis, P. Constantinou, and D. Vouyioukas, "Power angle profile measurements and capacity evaluation of a SIMO system at 60 GHz," in *Proc. 21st Annu. IEEE Int. Symp. Pers., Indoor Mobile Radio Commun.*, Sep. 2010, pp. 1027–1031.
[15] S. A. M. Tariq, C. Despins, S. Affes, and C. Nerguizian, "Statistical modeling of 60 GHz wireless channel in an underground mine gallery," in *Proc. IEEE Int. Conf. Ubiquitous Wireless Broadband (ICUWB)*, Montreal, QC, Canada, Oct. 2015, pp. 1–5.
[16] S. A. M. Tariq, C. L. Despinsi, S. Affes, and C. Nerguizian, "60 GHz temporal dispersion characteristics with different antenna polarizations in an underground mine," in *Proc. IEEE 28th Annu. Int. Symp. Pers., Indoor, Mobile Radio Commun. (PIMRC)*, Montreal, QC, Canada, Oct. 2017, pp. 1–5.
[17] S. A. M. Tariq, C. Despins, S. Affes, and C. Nerguizian, "Scattering effect based on measurements of reflection coefficients at 60 GHz in an underground mine gallery," in *Proc. IEEE 25th Annu. Int. Symp. Pers., Indoor, Mobile Radio Commun. (PIMRC)*, Washington, DC, USA, Sep. 2014, pp. 217–221.
[18] S. Ahsanuzzaman Md Tariq, C. Despins, S. Affes, and C. Nerguizian, "Rough surface scattering analysis at 60 GHz in an underground mine gallery," in *Proc. IEEE Int. Conf. Commun. Workshops (ICC)*, Jun. 2014, pp. 724–729.
[19] S. A. M. Tariq, "Characterization and modelling of scattered wireless channel at 60 GHz in an underground mine gallery," Ph.D. dissertation, Dept. Elect. Eng., Université de Montréal-École Polytechnique, Montreal, QC, Canada, 2016. [Online]. Available: https://publications.polymtl.ca/2289/
[20] A. Benzakour, S. Affes, C. Despins, and P.-M. Tardif, "Wideband measurements of channel characteristics at 2.4 and 5.8 GHz in underground mining environments," in *Proc. IEEE 60th Veh. Technol. Conf. (VTC-Fall)*, vol. 5, Sep. 2004, pp. 3595–3599.
[21] G. D. Durgin and T. S. Rappaport, "Theory of multipath shape factors for small-scale fading wireless channels," *IEEE Trans. Antennas Propag.*, vol. 48, no. 5, pp. 682–693, May 2000.
[22] M. Samimi, K. Wang, Y. Azar, G. N. Wong, R. Mayzus, H. Zhao, J. K. Schulz, S. Sun, F. Gutierrez, and T. S. Rappaport, "28 GHz angle of arrival and angle of departure analysis for outdoor cellular communications using steerable beam antennas in New York City," in *Proc. IEEE 77th Veh. Technol. Conf. (VTC Spring)*, Jun. 2013, pp. 1–6.
[23] M. Ndoh and G. Y. Delisle, "A modern approach to complex propagation problems in confined media," presented at the URSI Gen. Assem., Maastricht, The Netherlands, 2002, pp. 314–317.
[24] Y. Zhang, A. K. Brown, W. Q. Malik, and D. J. Edwards, "High resolution 3-D angle of arrival determination for indoor UWB multipath propagation," *IEEE Trans. Wireless Commun.*, vol. 7, no. 8, pp. 3047–3055, Aug. 2008.
[25] A. Forooshani, S. Bashir, D. Michelson, and S. Noghanian, "A survey of wireless communications and propagation modeling in underground mines," *IEEE Commun. Surveys Tuts.*, vol. 15, no. 4, pp. 1524–1545, 4th Quart., 2013.
[26] C. Garcia-Pardo, J.-M. Molina-Garcia-Pardo, M. Lienard, D. Gaillot, and P. Degauque, "Double directional channel measurements in an arched tunnel and interpretation using ray tracing in a rectangular tunnel," *Prog. Electromagn. Res. M*, vol. 22, pp. 91–107, 2012.
[27] A. E. Forooshani, S. Noghanian, and D. G. Michelson, "Characterization of angular spread in underground tunnels based on the multimode waveguide model," *IEEE Trans. Commun.*, vol. 62, no. 11, pp. 4126–4133, Nov. 2014.
[28] A. F. Molisch, *Wireless Communications*. Hoboken, NJ, USA: Wiley, 2010.
[29] D. Valchev and D. Brady, "Three-dimensional multipath shape factors for spatial modeling of wireless channels," *IEEE Trans. Wireless Commun.*, vol. 8, no. 11, pp. 5542–5551, Nov. 2009.
[30] S. J. Nawaz, N. M. Khan, and R. Ramer, "3-D spatial spread quantifiers for multipath fading wireless channels," *IEEE Wireless Commun. Lett.*, vol. 5, no. 5, pp. 484–487, Oct. 2016.